Structure, stability and water adsorption on ultra-thin TiO_2 supported on TiN

*José Julio Gutiérrez Moreno [1,2,3 *], Marco Fronzi [4,5], Pierre Lovera [3], Alan O'Riordan [3], Michael J. Ford [5], Wenjin Li [1 §], Michael Nolan [3†].*

[1] Institute for Advanced Study, Shenzhen University, Shenzhen 518060, China.
[2] Key Laboratory of Optoelectronic Devices and Systems of Ministry of Education and Guangdong Province, College of Physics and Optoelectronic Engineering, Shenzhen University, Shenzhen 518060, China.
[3] Tyndall National Institute, University College Cork. Lee Maltings, Dyke Parade, Cork, T12 R5CP, Ireland.
[4] International Research Centre for Renewable Energy, State Key Laboratory of Multiphase Flow in Power Engineering, Xi'an Jiaotong University, Xi'an 710049, Shaanxi, China
[5] School of Mathematical and Physical Sciences, University of Technology Sydney, P.O. Box 123, Broadway, Sydney, New South Wales 2007, Australia

Email: [*] juliogutierrez@szu.edu.cn, [§] liwenjin@szu.edu.cn, [†] michael.nolan@tyndall.ie

ABSTRACT

Interfacial metal-oxide systems with ultrathin oxide layers are of high interest for their use in catalysis. In this study, we present a density functional theory (DFT) investigation of the structure of ultrathin rutile layers (one and two TiO_2 layers) supported on TiN and the stability of water on these interfacial structures. The rutile layers are stabilized on the TiN surface through the formation of interfacial Ti–O bonds. Charge transfer from the TiN substrate leads to the formation of reduced Ti^{3+} cations in TiO_2. The structure of the one-layer oxide slab is strongly distorted at the interface, while the thicker TiO_2 layer preserves the rutile structure. The energy cost for the formation of a single O vacancy in the one-layer oxide slab is only 0.5 eV with respect to the ideal interface. For the two-layer oxide slab, the introduction of several vacancies in an already non-stoichiometric system becomes progressively more favourable, which indicates the stability of the highly non-stoichiometric interfaces. Isolated water molecules dissociate when adsorbed at the TiO_2 layers. At higher coverages the preference is for molecular water adsorption. Our ab initio thermodynamics calculations show the fully water covered stoichiometric models as the most stable structure at typical ambient conditions. Interfacial models with multiple vacancies are most stable at low (reducing) oxygen chemical potential values. A water monolayer adsorbs dissociatively on the highly distorted 2-layer $TiO_{1.75}$-TiN interface, where the Ti^{3+} states lying above the top of the valence band contribute to a significant reduction of the energy gap compared to the stoichiometric TiO_2-TiN model. Our results provide a guide for the design of novel interfacial systems containing ultrathin TiO_2 with potential application as photocatalytic water splitting devices.

1. INTRODUCTION

Titanium nitride (TiN) protective coatings are used in multiple technologies and applications including biomedical and surgical instruments, automotive and aerospace parts and sporting goods.[1-4] The widespread use of TiN comes from its capacity to enhance the hardness, resistance to corrosion and biocompatibility of other materials.[3-6] TiN is also used in microelectronic devices, due to its good conductivity and significant plasmonic performance[7] while it is a potential anti-biofouling coating for detectors that are designed to be exposed to harsh environments[6,8,9]. TiN films can be fabricated by widely-used deposition techniques[10] including magnetron sputtering,[5,11] ion-beam sputtering (IBS)[12], physical vapour deposition (PVD),[13-16], chemical vapour deposition (CVD)[17-19] or atomic layer deposition (ALD).[20,21]

TiN can be oxidised to produce a TiO_2 layer or scale when it is exposed to high temperatures or after long exposure times at ambient conditions[22-27]. The formation of a thin TiO_x layer on the nitride surface can deteriorate the adherence of the coating, which will affect the mechanical properties and resistivity to corrosion.[25,28,29]. However, there are other applications of such an interfacial system in which the growth of ultrathin TiO_2 films is precisely controlled and one example is in catalysis, where ultra-thin films can show potential for H_2O splitting[30,31], CO_2 reduction[32] or fixation of N_2 to NH_3.[33] In bulk TiO_2, doping or defect formation is needed to produce reduced Ti^{3+} sites, which can be difficult to control. By contrast, we have shown that in TiO_2-TiN interfaces, reduced Ti^{3+} states in TiO_2 are naturally formed as a result of charge transfer from TiN to TiO_2. The well-known reduced Ti^{3+} states lie in the middle of the TiO_2 energy gap. Thus, the controlled growth of TiO_2 on TiN could be further used for tuning the TiO_2 optical bandgap by oxide-nitride interaction, potentially leading to an optimized catalytic performance under visible light.[34-36]

The oxidation of TiN is a complex process and the structure of the resulting oxide will be highly dependent on the temperature and the thickness of the oxide layer. Ab initio molecular dynamics simulations[37] showed that at high temperatures, an ordered and non-defective crystalline TiO_2 structure tends to form on the TiN surface. The difficulty in adsorbing oxygen after formation of TiO_2 layers can prevent further TiN oxidation. At low temperatures, defects can remain trapped inside the interface.[37] From experiments, it is observed that TiN deposited by CVD on Si (100) forms a uniform film with stoichiometric composition and predominance of (200) out-of-plane orientation at deposition temperatures in the range of 400-700 ℃.[38] The epitaxial growth of TiO_2 on TiN leads to the formation of rutile TiO_2 (110) with the presence of an interfacial oxynitride (TiN_xO_y) transition layer.[39]

In a previous publication,[40] we used Hubbard corrected density functional theory (DFT+U) to study the structure and electronic properties of rutile TiO_2 (110)–TiN (100) interfaces. We have found that in the rutile (110)–TiN interface system defects such as Ti vacancies in TiN, O vacancies in TiO_2 or interdiffusion of O and N atoms within the interface may be present. We observed the formation of Ti^{3+} cations, preferentially located in the interface region, which originate from charge transfer to TiO_2 upon interface formation or from the introduction of O vacancies in non-stoichiometric systems.

TiO_2 is one of the most extensively investigated metal oxides[41-46] and the wettability of TiO_2 can be tuned by surface morphology modifications or UV irradiation enhancing the hydrophilic features of the surface for its use as antibiofouling or self-cleaning coating material.[47-49] The multitude of TiO_2 applications and the ubiquitous presence of water explains the great interest in studying the interaction of water with different TiO_2 surfaces.[41,50,51] Water adsorption on TiO_2 can be described either as molecular or dissociative; in the latter surface hydroxyls result from the dissociation of H_2O into OH + H.[50,52] Most experimental works agree that water adsorbs molecularly at a pristine rutile (110) surface and dissociation may take place on site defects and step edges.[41,50,53] Nevertheless, there still remains some controversy from theoretical studies on water adsorption at pure TiO_2 and the results can be highly dependent on the simulation setup parameters, e.g. slab thickness, surface coverage or exchange-correlation functional.[41]

When the oxide layer on TiN grows above a certain thickness, the resulting oxide can be considered as pure TiO_2 and the surface morphology will not be affected by the substrate material. In our previous work,[54] we showed that when water is adsorbed on the rutile surface of TiO_2–TiN interfaces with a 4 O-Ti-O tri-layer thick oxide (11.10 Å), this behaves similarly to pure TiO_2. We found that at ambient O_2 and H_2O pressures the interface is fully covered with molecular water. Isolated water molecules tend to dissociate on the rutile surface, although these are stable only at very low H_2O pressures. These results are in line with a previous DFT study of water adsorption on pure rutile (110) by Kowalski et al.[55] This work also found the preferential dissociative adsorption for an isolated water molecule. Molecular water is more stable at higher surface coverages, whereas the small energy differences between molecular and dissociative adsorption modes at partially covered surfaces suggest the likely formation of molecular H_2O islands where the molecules at the boundary may dissociate.

The increasing interest in metal-oxide interfacial systems lies in the fact that the activity of an ultra-thin oxide and can be significantly altered by the characteristics of the substrate. This effect can be explained as a result of the lattice distortion that the oxide requires to match the substrate's lattice parameters combined with potential charge transfer that takes place in the metal-oxide interface. As an example, previous studies on single water molecule adsorption at ultra-thin MgO (100) supported on Ag (100)[56,57] and Mo (100)[58] found enhanced water adsorption and reduced dissociation barriers on the interfacial systems when compared to the extended MgO (100) surface. This preference for dissociated water has its origin in the interfacial tensile strain that causes an expansion of the MgO lattice, which facilitates the dissociation of water. Charge-transfer effects are not considered as crucial.[56] [58] Nevertheless, theoretical studies on molecular adsorption at oxide-metal interfaces still remain scarce. As far as we are aware, the only first principles study on water adsorption TiO_2-TiN interfaces as a model of oxidised TiN is our recently published work.[54]

Therefore, with limited knowledge of the structural and electronic properties of ultrathin TiO_2 supported on TiN, we present in this paper a detailed investigation of TiO_2-TiN interfaces with 1 and 2-layer rutile TiO_2 (110), with the aim to understand how the resulting interface properties are affected by the thickness of the deposited oxide. We applied Hubbard-Corrected Density Functional Theory (DFT+U) simulations to account for potential reduced Ti^{3+} states in the oxide layer. We discuss the structural and electronic properties of ultra-thin TiO_2 on TiN, including the formation of defects in the interfacial region and on the oxide surface. Finally, we present a systematic study of water adsorption and coverage on the ultrathin TiO_2 layer at TiN. Based on ab initio atomistic thermodynamics analyses, we discuss the thermodynamic stability of water adsorbed at the oxide-nitride system at realistic temperatures and within a range of oxygen and water pressure conditions. The simulations carried out provide a comprehensive insight into the structural and electronic properties of ultrathin TiO_x supported on TiN, presenting this interfacial system as a promising interface for catalysis. The main outcomes of this study can be used as a guide for the rational design of novel catalysts containing ultra-thin TiO_2.

2. COMPUTATIONAL DETAILS

We carried out periodic Density Functional Theory (DFT) calculations within the framework of the Vienna Ab Initio Simulation Package (VASP). The projector augmented-wave (PAW) potentials[59,60] are used to describe the core-valence interaction, with the valence electrons described by periodic plane waves with cut-off energy of 400 eV. We used the generalized gradient approximation (GGA) for the exchange-correlation functional as formulated by Perdew and Wang (PW91).[61] The convergence criteria used for energy and forces on each atom and 10^{-4} eV and 0.02 eV/Å respectively. All the calculations in this study include a correction for on-site Coulomb interactions (DFT+U) [62], with U = 4.5 eV applied on the Ti 3d electrons in TiO_2. This correction is applied to account for the potential reduction of Ti atoms that can form in the TiO_2-TiN interface. The U value was chosen in consistency with our previous works on TiO_2-TiN interfaces[40,54] and surface modified TiO_2.[63] We use Bader charge analysis[64] to assess the localization of reduced Ti cations.

We calculated the equilibrium lattice for the bulk TiN (a = 4.26 Å) and rutile TiO_2 (a = 4.64 Å; c = 2.97 Å) using a Monkhorst-Pack sampling grid of (14 x 14 x 14) k-points and (4 x 4 x 4) k-points respectively. Rutile TiO_2 (110) and TiN (100) surfaces have the lowest surface energy for their respective polymorphs and compositions.[65,66] Upon cleaving from the bulk, the 5-layer thick (10.66 Å) rock-salt TiN (100) surface is composed of neutral planes, each with TiN stoichiometry. The 1-layer and 2-layer thick O–Ti–O tri-layer TiO_2 slabs have an approximate thickness of 2.78 Å and 5.55 Å respectively, and exhibit rutile (110) surface structure before relaxation. A vacuum thickness about 18 Å was introduced between the interface slabs to avoid interactions along the normal between the opposite sides of the model interface. The TiN (100) supercell surface model has 120 atoms and lattice parameters of a = 8.51 Å; b = 12.77 Å. The stoichiometric rutile TiO_2 (110) 1-layer and 2-layer thick surfaces contain 36 and 72 atoms respectively, with equilibrium lattice dimensions of a = 8.92 Å; b = 13.12 Å. We use a (2x1x1) Monkhorst-Pack sampling grid during ionic relaxation. After convergence is achieved, we run single point calculation with a (6x4x1) grid to obtain a more accurate electronic density of states (EDOS) for the pristine interfaces. Methfessel-Paxton smearing function with σ = 0.1 eV was employed to integrate the Brillouin Zone

The interfacial binding energy is estimated from the difference in energy between the equilibrium TiN free-standing slab, the compressed TiO_2 slab (at the interface lattice constant) and the total energy of the TiO_2-TiN interface. In addition to the perfect TiO_2-TiN stoichiometric system, we also considered the formation of off-stoichiometric systems arising from the formation of O and Ti vacancies. The O vacancy formation energy, normalized by the number of vacancies, is given by the following expression

$$E(O)_{vac} = (E_{defective} - E_{stoichiometric} - n \cdot E_{O_2}/2)/n \quad (1)$$

Where $E(O)_{vac}$ is the vacancy formation energy, $E_{defective}$ is the total energy of the relaxed system after the vacancy formation, $E_{stoichiometric}$ is the total energy of the initially non-defective interface, n is the number of vacancies introduced in the system and the $E_{O_2}/2$ term corresponds to one half of the total energy of an isolated O_2 molecule. The Ti vacancy formation energy is calculated by an analogous expression, in which $E_{O_2}/2$ is substituted by the energy of a single Ti atom within a bulk hexagonal close-packed (hcp) lattice. The energy of an isolated O_2 molecule was calculated using a Γ-point sampling grid, an orthogonal supercell with sides larger than 15 Å to avoid molecule self-interaction and the same plane wave cut-off and convergence criteria as the slabs.

The adsorption of water was simulated by the deposition and further relaxation of H_2O molecules at low coordinated Ti sites on the TiO_2 surface. Water dissociation (hydroxyl) was created by binding one hydrogen atom from water near the closest low coordinated surface O site. The adsorption energies (E_{ads}) per adsorbed water were computed for molecular and dissociative adsorption modes using the following expression:

$$E_{ads} = (E_{hydrated} - E_{surf} - n \cdot E_{H_2O})/n \quad (2)$$

Where E_{surf} and $E_{hydrated}$ are the total energy of the system before and after the adsorption of water respectively. The energy of a single water molecule is multiplied by the number of waters in the system (n). As for molecular oxygen, the energy of an H_2O molecule was calculated using the same supercell, Γ-point sampling grid and 400eV plane wave cut-off.

To analyze the relative thermodynamic stability of the interface models in a realistic environment, we use the DFT-derived total energies as input into an atomistic thermodynamics framework. Here, we assume that the interfaces are in equilibrium with two infinite gas reservoirs (i.e. O_2 and H_2O) that can exchange particles with no change in their chemical potential. This allows us to include in the effect of the surrounding gas phase in thermodynamic equilibrium with the surface. The interface energy can then be calculated as follows:

$$\gamma(p,T) = 1/A[G - \sum N_i \mu_i(p,T)] \quad (3)$$

where A is the interface area; G is the Gibbs free energy of the crystal; $\mu(p,T)$ is the chemical potential of the atomic species in i the system; and the term N_i is the total number of atoms of species i. We assume that O_2 and H_2O

reservoirs are in non-equilibrium with each other. Therefore, we can plot the interface energy as a function of the species of interest by treating the chemical potentials as independent variables, so that a broad spectrum of environmental conditions can be treated. Furthermore, by approximating water vapour and oxygen as ideal gases, we explicitly
introduce pressure and temperature in our model through the analytic relation between chemical potentials and the temperature and pressure of the two gas reservoirs as follows:

$$\mu_O(p,T) = \left[\frac{1}{2}E_{O_2} + \mu'_{O_2} + k_B T ln\left(\frac{p_{O_2}}{P^0}\right)\right] \quad (4)$$

$$\mu_{H_2O}(p,T) = \left[E_{H_2O} + \mu'_{H_2O} + k_B T ln(\frac{p_{H_2O}}{P^0})\right] \quad (5)$$

Here, T and p represent the temperature and partial pressure of the two gases, p^0 denotes atmospheric pressure and k_B is the Boltzmann constant. μ' is the energetic term that includes contributions from rotations and vibrations of the molecule, as well as the ideal-gas entropy at 1 atm which can be calculated or taken from experimental values listed in thermodynamic tables.[67] A more detailed description of the methodology can be found in our previous works.[54,68,69]

3. RESULTS AND DISCUSSION

3.1 Structure of ultra-thin TiO_2 on TiN substrate

The DFT optimized lattice constants for the bulk cubic rock-salt structure TiN (a = 4.26 Å) and the tetragonal rutile TiO_2 ($a = b$ = 4.64 Å and c = 2.97 Å) are used to generate the TiO_2 (110) and TiN (100) surface models. Rutile TiO_2 (110) and TiN (100) are the most stable low-index crystal cuts for rutile TiO_2[21] and TiN.[46, 66] The rutile TiO_2 (110) structure exhibits two types of oxygens on the surface: the two-fold coordinated oxygen (O_{2f}), that bridge two Ti atoms on the surface, and the three-fold coordinated oxygens (O_{3f}). There are also two types of surface Ti: the five-fold coordinated (Ti_{5f}) and the six-fold coordinated (Ti_{6f}) which is bridged by two bridging O_{2f} and these alternate along the [001] direction.

To minimize the lattice mismatch between both surfaces, a rutile (110) (3x2) surface supercell, with equilibrium lattice constants a = 8.91 Å; b = 13.12 Å was generated and compressed in-plane to match the TiN (100) (2x3) surface supercell with lattice parameters of a = 8.51 Å; b = 12.77 Å, which minimises the lattice strain in TiO_2. In our approach, the oxide grows on the TiN and thus it has to accommodate to the substrate structure. The interface with 1-layer thick TiO_2 was generated by removing one O-Ti-O tri-layer from the 2-layer thick model. This approach was chosen to start with a better initial estimation of the nitride-oxide interfacial bond distances. By minimizing the distortions due to lattice mismatch, we can expect to obtain a more stable TiO_2 monolayer.

More details on the construction of the interfaces and the structural and electronic properties of TiO_2 (110)–TiN (100) interfaces can be found in a previous publication.[54]

Figure 1 shows the structure of the 1-layer and 2-layer thick TiO_2 (110)–TiN (100) interfaces. Surface Ti atoms on the TiN slab migrate from their initial positions on the surface to bind with oxygen, leading to the formation of multiple Ti-O interfacial bonds that will promote interface stability.[54] We do not observe structural changes in the subsurface TiN layers. The calculated adhesion energies for the deposition of the compressed TiO_2 slab on TiN are -3.22 eV, which correspond to 0.40 eV per Ti-O interfacial bond, for the 1-layer slab; and -1.66 eV, corresponding to 0.33 eV per bond, for the 2-layer slab.

The formation of reduced Ti^{3+} cations in the oxide is assessed by computing Bader charges. The charge transfer to TiO_2 forms reduced Ti^{3+} cations that are indicated by light green atoms in Figure 1. In the 1-layer model, we find computed Bader charges of between 1.32-1.35 electrons for Ti^{4+} sites and between 1.72-1.80 electrons for the Ti^{3+} atoms in TiO_2. In the 2-layer structure, the computed Bader charges range between 1.28-1.33 electrons for Ti^{4+} sites and 1.67-1.77 electrons for the reduced Ti^{3+} sites. The spin magnetizations of Ti^{3+} centres in both models have absolute values of 0.9 μ_B.

The 1-layer thick TiO_2 in Figure 1(a) relaxes into a highly distorted structure when interfaced with the TiN surface. Surface Ti atoms in TiN migrate by up to 0.7 Å from their initial position to bind with O atoms upon interface formation. The oxide layer covers the entire TiN surface and, typically for such

thin layers[70,71], it does not preserve the symmetry present in the rutile (110) structure. From the top view, we observe hexagonal-like patches that resemble a flattered rutile (100) geometry surface and the oxide is clearly distorted. The formation of highly disordered structures has been observed in other ultra-thin TiO_2 films supported on metal surfaces including Ag (100)[70] or Ni (100).[71] In the oxide slab, five out of the six reduced Ti^{3+} are undercoordinated five-fold (Ti_{5f}) species and the remaining Ti^{3+} is six-fold (Ti_{6f}) coordinated. For the non-reduced Ti^{4+}, one half are Ti_{6f} coordinated to neighbouring O and the remaining three titanium bind to up to five oxygen atoms. The reduced Ti^{3+} atoms in the oxide are aligned along the equivalent $[1\bar{1}0]$ direction and localized on the Ti species that would correspond to Ti_{5f} atoms on an undistorted crystalline single layer rutile (110). The high concentration of Ti^{3+} (half of the total Ti atoms in the oxide), with larger atomic radii compared to Ti^{4+}, along with the compression applied to TiO_2 to compensate the lattice mismatch with TiN may explain the significant distortions and the formation of this non-ordered oxide monolayer.

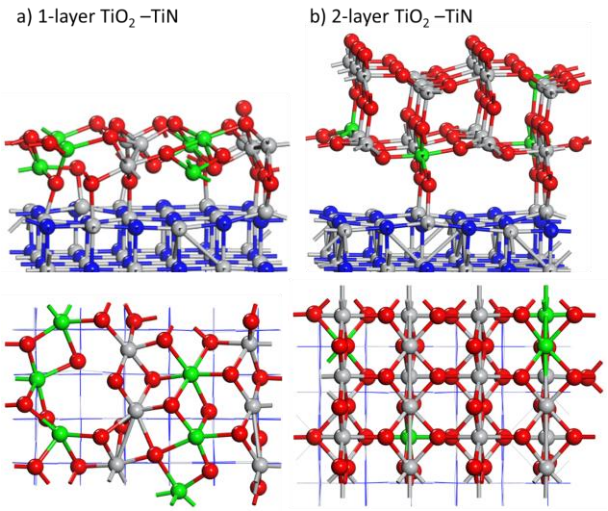

Figure 1. Structure of the stoichiometric rutile TiO_2 (110)–TiN (100) interface models. The figures show the front perspective and top view of (a) interface with 1-layer thick TiO_2 and (b) interface with 2-layer thick TiO_2. Reduced Ti^{3+} atoms in TiO_2 represented by green spheres, Ti^{4+} atoms in TiO_2 and all Ti in TiN are grey, N atoms are blue and O atoms are red.

In the 2-layer thick model (Fig.1(b)) the rutile (110) structure is clearly preserved. The migration of Ti from the nitride towards the oxide is between 0.3 and 0.8 Å upon interface relaxation. The TiO_2 octahedra rotate perpendicularly to the [001] axis, due to the strain applied to compensate the lattice mismatch with TiN along with the presence of reduced Ti^{3+} centres, which are preferentially located in the interfacial region. The features observed in the structure of 2-layer thick TiO_2 - TiN interfaces are consistent with our previous model with a thicker oxide layer.[40]

3.2 Defects in TiO_2-TiN interface models

In this section we increase the complexity of the interface models and examine the structural stability of non-stoichiometric structures, starting from perfect one and two-layer TiO_2-TiN interfaces. Previous experimental studies have detected that defects can arise during oxide growth and will, therefore, affect the properties of metal-oxide interfaces.[11, 19] We discuss the formation of O vacancies[72] in TiO_2, which can be created by thermal annealing and is the most common defect in other metal-oxides. We also evaluate the presence of Ti vacancies in TiN that can form due to surface Ti migration on the TiN surface when this is in contact with atmospheric O_2.[37,39]

Figure 2 shows the structure and energy cost for the formation of the most stable O vacancies in the 1-layer thick oxide model. Figure 2(a) shows the structure of the stoichiometric interface along with the suggested transition pathway towards the formation of the O-defective system. We performed relaxations on different model structures to find the most energetically favourable defect sites. The O vacancy site, indicated in yellow, is the most stable vacancy site among many possible vacancies, and its vacancy formation energy cost is only 0.51 eV with respect to the perfect interface. Upon relaxation of the defective system, one of the oxygen atoms nearest the vacancy (labelled as O^1 in Figure 2(a)) migrates to occupy the vacant site above a surface Ti on the TiN surface. The O atoms that are neighbours of $Ti^{1'}$ (namely O^1, O^2 and O^3) go through relaxation following the transition path indicated with red arrows in Figure 2(a). The introduction of an oxygen vacancy does not lead to the formation of extra Ti^{3+} in the oxide, as can be expected from the absence of an O^{2-} anion. In this case, the creation of an O vacancy in an already

highly reduced oxide slab tends to favour delocalization (with computed Bader charges of 1.41 electrons, which signifies partial reduction) and the extra electrons are therefore evenly distributed around the oxide.

Given the low cost for the formation of the first oxygen vacancy, we also discuss the formation of a second O vacancy (Figure 2(c)). Taking as initial structure the system in which the first vacancy was created (Figure.2(b)), we found O^2 to be the most stable O-vacancy site on the oxide's surface. The formation energy for the second O vacancy is significantly increased, with a computed formation energy of 3.89 eV with reference to the single O-vacancy structure. The addition of two more electrons in an already highly reduced system, in which further relaxation could be hindered, can explain the high energy cost for the second O vacancy. We do not observe a significant distortion in the system produced by this second O vacancy despite the further reduction that arises in the oxide from the vacancy.

The computed Ti vacancy formation energy in TiN interfaced with the 1-layer thick oxide is as high as 4.62 eV, therefore we do not consider this defective interface for further study. The structure of the 1-layer interface with a Ti vacancy is discussed in the supporting information, Figure S1.

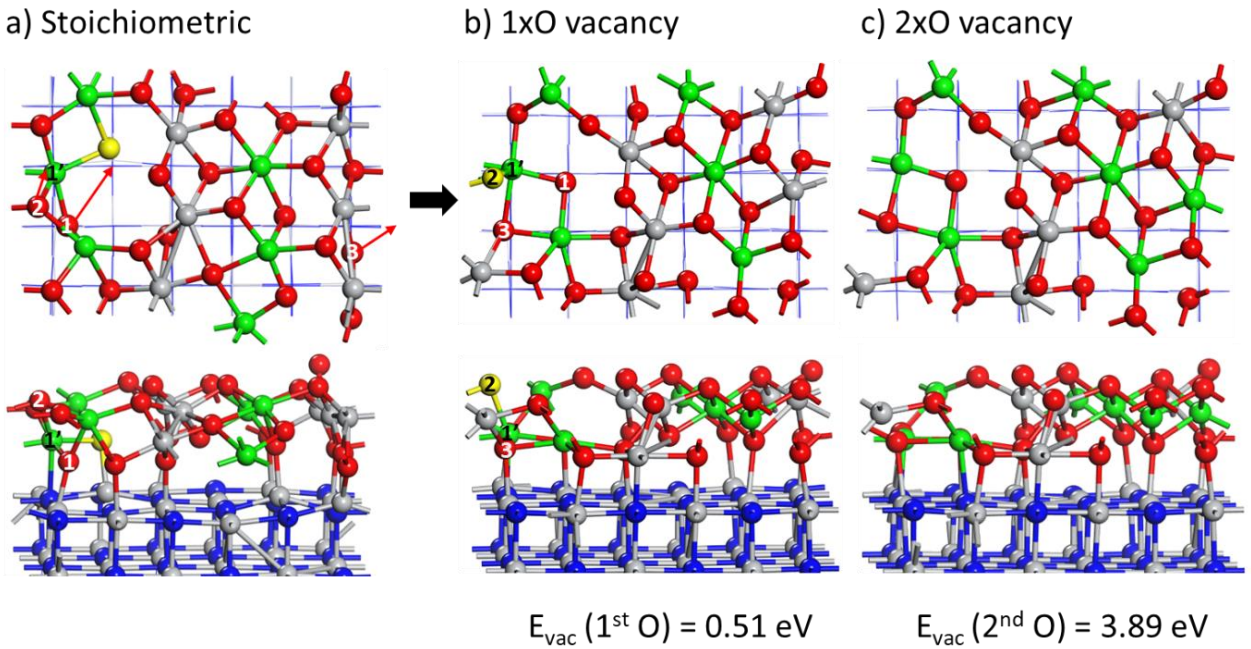

Figure 2. Structure of the O-defective 1-layer thick rutile TiO_2 (110)–TiN (100) interface models. We present (a) the initial stoichiometric model with arrows indicating the suggested transition pathway towards the formation of (b) the system with one oxygen vacancy; (c) shows the interface with 2xO vacancies. The figures for the non-stoichiometric systems show the front perspective and top view of the interfaces. The oxygen vacancy sites are represented in yellow, reduced Ti^{3+} atoms in TiO_2 are represented by green spheres, Ti^{4+} atoms in TiO_2 and all Ti in TiN are grey, N atoms are blue and O atoms are red.

Figure 3 shows the relaxed structure of 2-layer TiO_2-TiN interfaces with one O vacancy. We differentiate between vacancies created in (a) the terminating surface layer or (b) in the interfacial region. We computed formation energy values of 4.06 eV for an O_{2f} bridging surface oxygen vacancy in the terminating layer and 3.85 eV for an interfacial vacancy bridging TiO_2 and TiN. The calculated O vacancy energy values are slightly larger than those in the 4-layer thick rutile (110) - TiN model (3.40 eV at the interface) or a surface O vacancy in perfect rutile (110) surface (3.66 eV)[73], while the energy is more favourable than the formation of O vacancies in bulk rutile (E_{vac} = 4.4 eV).[74] The two non-stoichiometric structures are stable, and the rutile structure does not show

significant distortions after the vacancy formation. Although the difference in energy between these two models is quite small, we should take into account that surface defects may form from initially perfect interface under certain ambient conditions like the exposure to high temperatures while interfacial defects are most likely to arise and remain trapped upon oxidation of TiN.

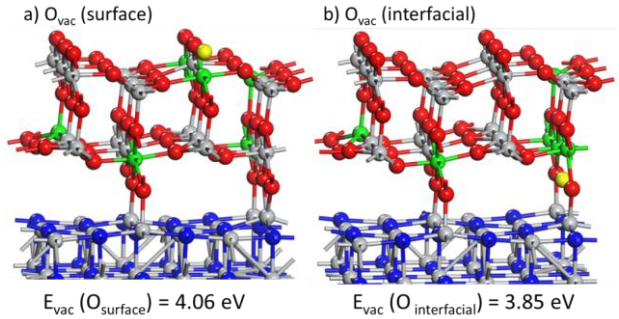

Figure 3. Structure of the O-defective 2-layer thick rutile TiO_2 (110)–TiN (100) interface models with (a) one surface O vacancy and (b) interfacial O vacancy. Figures on the top panel represent the frontal perspective view, the top view is shown on the bottom panel and the vacancy formation energy calculated taking as reference molecular O_2 is given below the figures. In the figure, the oxygen vacancy sites are represented by yellow spheres, reduced Ti^{3+} atoms in TiO_2 are represented are green, Ti^{4+} atoms in TiO_2 and all Ti in TiN are grey, N atoms are blue and O atoms are red.

In our previous study, we found that the introduction of several O vacancies becomes more favourable, leading to the stability of highly non-stoichiometric systems.[40] Based on these results, in addition to the single vacancy system in the 2-layer thick TiO_2 model, we also consider the formation of highly non-stoichiometric interfaces, in which all of the bridging O are removed from the interface region. Figure 4 depicts the structure of 2-layer thick interface models with 6 interfacial oxygen vacancies, which results in an interface with the oxide composition of $TiO_{1.75}$-TiN.

We considered two different approaches to generate this defective interface to explore the effect of different structures. The **etched model** in Figure 4(a) was generated by removing the 2 outermost O-Ti-O tri-layers from a 4-layer thick TiO_{2-x}-TiN model that already contained 6 oxygen vacancies ($TiO_{1.88}$-TiN). The initial structure of this interface is available in the Nomad repository.[75] The interface in Figure 4(b) (denoted the **slab model**) was generated by removing all the interfacial bridging oxygen in the perfect model from Figure 1(b). Both highly defective structures are stabilized by the formation of multiple Ti-O bonds within the interfacial region upon relaxation. In the **etched model,** the symmetry of rutile (110) structure is preserved on the surface, with a strongly distorted TiO_2 layer in the interfacial region, where some atoms occupy an interstitial-like position within the rutile structure. The **slab model** forms a highly distorted non-ordered oxide structure in which the crystalline patterns of the rutile structure are hardly identifiable. The total energy of the model with non-ordered TiO_{2-x} more stable than the etched oxide structure by 7.8 eV. This higher stability originates from multiple interfacial Ti-O bonds formed in the **slab model** upon DFT relaxation, compared to the **etched** interface, and indicates that distorted TiO_2 layers are more stable.

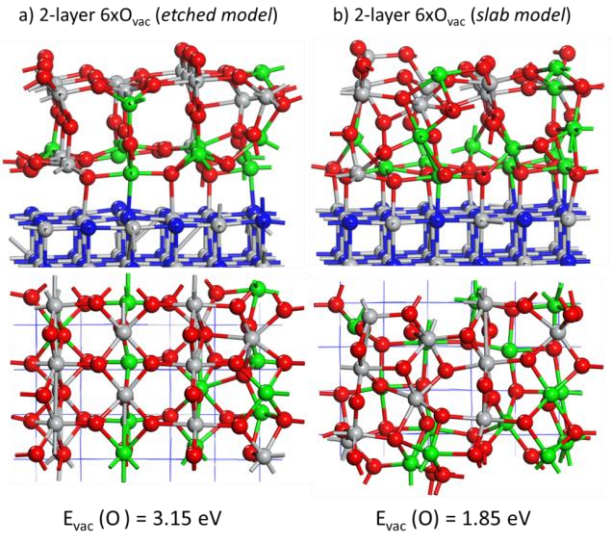

Figure 4. Structure of the 2-layer thick rutile TiO_2 (110)–TiN (100) interface models with 6 oxygen vacancies in the interface. The two different models are created by (a) removing 2 O-Ti-O tri-layers from the 4-layer thick models from reference[40], **etched model,** and (b) introducing 6 interfacial O vacancies in the 2-layer thick model in Figure 1.b, **slab model**. Figures on the top panel represent the frontal perspective view, the top view is shown on the bottom panel and the vacancy formation energy calculated taking as reference molecular O_2 is given below the figures. In the figure, the oxygen vacancy sites are represented by yellow spheres, reduced Ti^{3+} atoms in TiO_2 are represented are green, Ti^{4+} atoms in TiO_2 and all Ti in TiN are grey, N atoms are blue and O atoms are red.

We identify 14 reduced Ti^{3+} cations in the non-ordered oxide compared to 11 Ti^{3+} sites in the

etched model. The formation of extra reduced cations is expected after the introduction of many O vacancies and certainly influences the distortions in the rutile structure.

The formation energy of the O vacancies in the stoichiometric TiO_2-TiN model, to form the $TiO_{1.75}$-TiN system, is 3.15 eV / O_{vac} in the **etched** structure and 1.85 eV / O_{vac} in the **slab model**. The introduction of multiple vacancies in an already non-stoichiometric system has a lower energy cost compared to the formation of the first O vacancy at the stoichiometric system ($E_{vac} \geq 3.85$ eV). The suggested stability of the highly non-stoichiometric interfaces is consistent with our previous study, although our energy values are higher than the formation of the non-stoichiometric $TiO_{1.82}$-TiN system in an interface with 4-layer thick oxide (1.30 eV / O_{vac}).[40]

Despite the large difference in energy between the etched and slab models, both crystalline and disordered TiO_2 models can be stabilized and even coexist depending on the growth temperatures and techniques. In particular, it has been shown in a previous ab initio molecular dynamics work that at high temperatures, an ordered oxide structure can grow on the TiN surface, while at low temperatures vacancies and defects are prone to remain trapped inside the oxide structure.[37] We should note that although our approach considers the formation of vacancies from a perfect interface, the most likely origin of defect formation is during oxide growth and these defects can be trapped in the interface after the TiO_x growth of TiN and subsequently affect the structure and electronic features of the interfacial system.

3.3. Water adsorption at ultra-thin TiO_2 models on TiN

3.3.1 Adsorption of one water molecule

Water is present in nearly every environment and can interact with metal oxide surfaces such as TiO_2. Therefore, it is important to understand how the presence of water can alter fundamental properties of TiO_2 films. In the present section, we discuss the adsorption of water on the previously described oxide-nitride interfaces, including stoichiometric TiO_2 and several O-defective TiO_{2-x} models supported on TiN.

In the interfaces where the usual rutile (110) surface termination is clearly present, such as the stoichiometric 2-layer TiO_2-TiN interface, the water molecules are adsorbed on top of a surface Ti_{5f} site, which is the most favourable adsorption site on rutile (110) surfaces.[41] For the interfaces with highly distorted surface terminations, the water molecules were systematically deposited at different under-coordinated Ti atoms exposed on the surface, searching for the most stable adsorption site. For the dissociative adsorption of water, a hydroxyl (OH) from water is kept on the same site as molecular H_2O was adsorbed and the second hydrogen is adsorbed at an adjacent O_{2f} site.[41] We also discuss the stability of molecular water against dissociated, hydroxyl adsorption modes for an isolated H_2O which is equivalent to 1/6 monolayer (ML) coverage, and for fully-covered surfaces (1 ML coverage) on TiO_2–TiN interface models.

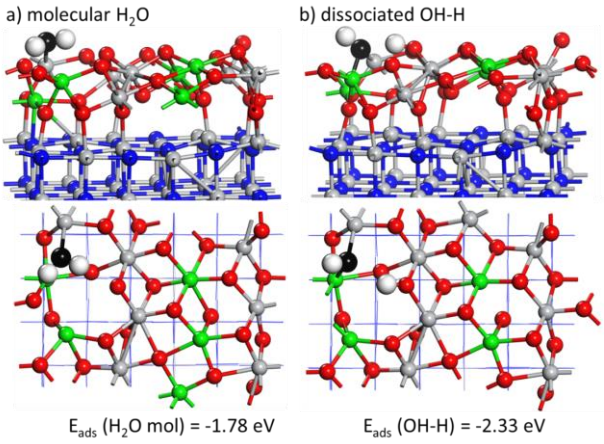

Figure 5. Structure of isolated (a) molecular water (H_2O) and (b) dissociated water (OH-H) adsorbed at stoichiometric 1-layer thick TiO_2 -TiN interface. The adsorption energy values are presented under figures. The Ti^{3+} atoms in TiO_2 are represented by green spheres, Ti^{4+} atoms in TiO_2 and all Ti in TiN are grey, N atoms are blue, O atoms from TiO_2 are red, O atoms from adsorbed water are black and H atoms are white.

The computed adsorption energy per water molecule, for molecular and dissociated water adsorption at the different TiO_2-TiN interfaces as a function of the water surface coverage are presented under the relaxed structure figures and summarized in Table S1. The distances for the bonds formed between the rutile surface and the

adsorbed species are listed in the supporting information section (Table S2).

The most stable configuration for one isolated water adsorbed on stoichiometric 1-layer thick TiO_2-TiN interface is shown in Figure 5. The negative energy indicates that molecular adsorption is favourable, with E_{ads} = -1.78 eV. The dissociation of water contributes to the further stabilization of the model by 0.55 eV, with E_{ads} = -2.30 eV. The bond formed between the adsorbed O and the surface Ti is 2.23 Å for water and 2.05 Å for the hydroxyl.

The adsorption of isolated water on the O-defective 1-layer TiO_2–TiN interface (Fig.S2), where H_2O is adsorbed with its O sitting at the vacancy site, behaves similarly to the stoichiometric model. Our results show the preferred dissociation of isolated water on the defective TiO_2 layer, with computed adsorption energies of -1.17 eV for molecular and -1.73 eV for dissociated water. The stronger adsorption energy for dissociated water at the stoichiometric TiO_2 layer is different from the preference for dissociative water adsorption on defective rutile (110) [53,76], however our interface model exhibit a distorted geometry in which the surface layer is also different from that of pure rutile (110) and has a larger number of reduced Ti^{3+} species.

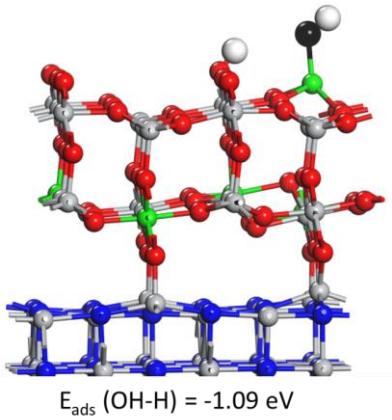

Figure 6. Structures of a single (OH-H) on perfect 2-layer thick rutile (110) TiO_2 -TiN interface. The adsorption energy is presented under the figure. The Ti^{3+} atoms in TiO_2 are represented by green spheres, Ti^{4+} atoms in TiO_2 and all Ti in TiN are grey, N atoms are blue, O atoms from TiO_2 are red, the O atoms from adsorbed water is black and H atoms are white.

On the 2-layer thick stoichiometric TiO_2-TiN interface (figure 6), the preference for an isolated water is dissociative adsorption (E_{ads} (OH-H) = -1.09 eV) and this is 0.41 eV more stable than the adsorption of molecular H_2O. The adsorption of dissociated water produces a strong distortion on the rutile layer where the Ti migrates outwards by ca. 1.6 Å with respect to its initial position on the bare layer and binds with the OH group.

Adsorption of isolated molecular water at the defective 2-layer $TiO_{1.75}$-TiN interfacial systems (with all interface oxygen removed), using equation (2) from the methodology section results in endothermic adsorption of 1.24 eV on the **etched** model and 1.54 eV on the **slab** oxide interface model. The adsorption energy is usually employed as a quantitative description of the new bonds created between the surface and the adsorbates. However, in our case, the total adsorption energy of water is also influenced by a contribution from the atomic relaxations in the TiO_2-TiN interface after water is adsorbed, as previously described in Ref[54]. The reference for the energy calculation is the total energy of the initially bare interface model. To estimate the influence that the distortions on the rutile-TiN interface have on E_{ads}, we define the distortion energy (E_{dist}) as the difference in energy between the pristine interface model (before molecular adsorption) and the relaxed structure after water desorption. If the corresponding E_{dist} is subtracted to the adsorption energy computed taking the pristine surface as a reference; we can get an estimation of the energy of the bonds formed between water and the oxide interface.

Both $TiO_{1.75}$-TiN interfaces with isolated H_2O exhibit adsorption energies that are strongly influenced by the interfacial atomic relaxations, which are responsible for an increase in the total energy by 2.33 eV on the **etched model** and 2.52 eV in the **slab oxide model**. These values give insights into the strong distortions produced on the oxide layer after water adsorption, which is clear in Figures 7 and 8. On the **etched model** (Figure 7), dissociative adsorption of H_2O, with an adsorption energy of -1.73 eV, is more stable than the molecular mode, for which the adsorption energy is -0.79 eV; these are the adsorption energies using the model of the interface described in the previous paragraph as a reference. The adsorption of water

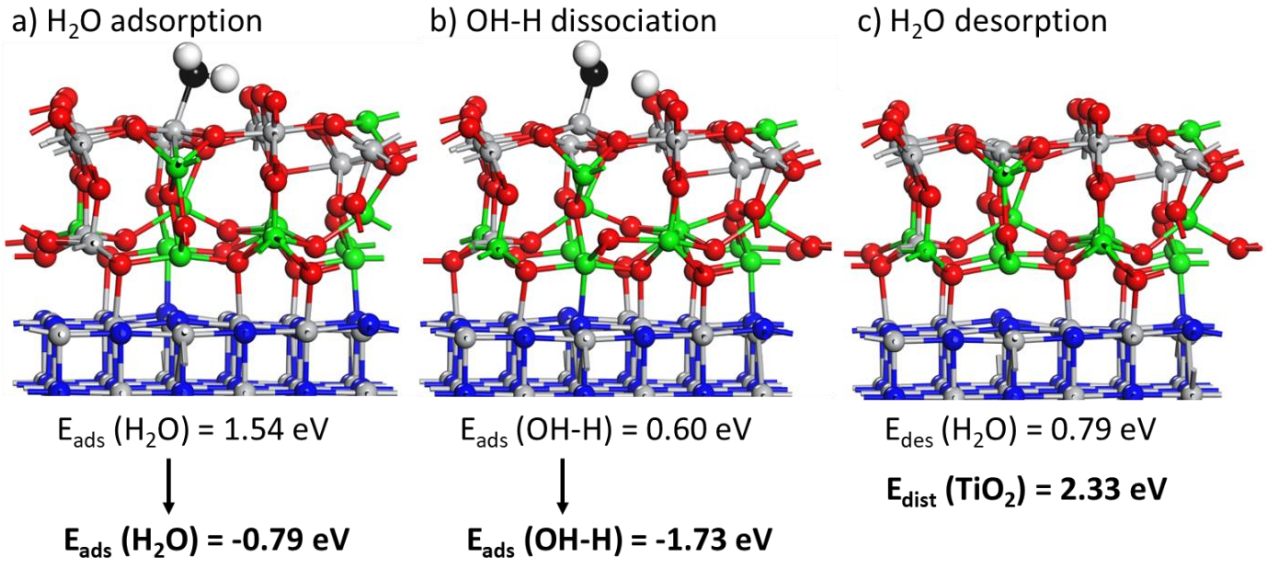

Figure 7. Structure of (a) molecular water (H_2O) adsorption, (b) dissociated water (OH-H) adsorption and (c) water desorption at the 2-layer thick **etched model** of rutile (110) surface on TiO_2 -TiN interfaces. The adsorption energy values using the pristine surface as reference (equation 2) is presented directly under (a) and (b) figures. The water desorption energy (E_{des}) and the distortion energy (E_{dist}), that shows the energy cost for the distortion produced in the original interface and after removing water, are presented under figure (c). The corresponding E_{ads} using the distorted surface (higher energy) as reference are presented in bold and linked with arrows below (a) and (b). The interface structures are represented following the same colour code as the previous figures.

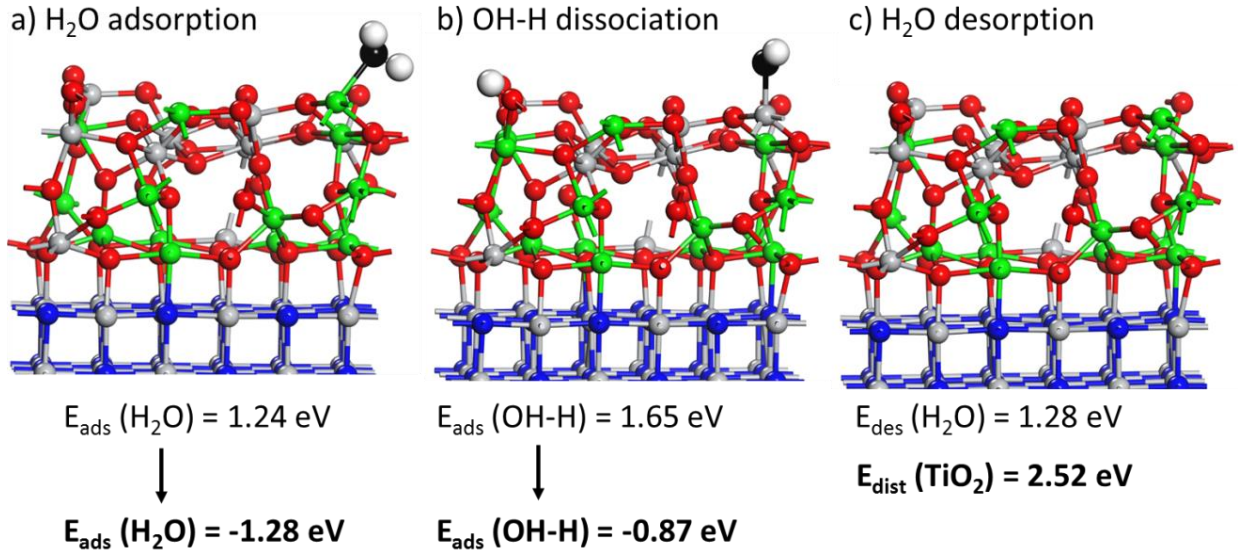

Figure 8. Structure of (a) molecular water (H_2O) adsorption, (b) dissociated water (OH-H) adsorption and (c) water desorption at the 2-layer thick **slab model** of rutile (110) surface on TiO_2 -TiN interfaces. The adsorption energy values using the pristine surface as reference (equation 2) is presented directly under (a) and (b) figures. The water desorption energy (E_{des}) and the distortion energy (E_{dist}), that shows the energy cost for the distortion produced in the original interface and after removing water, are presented under figure (c). The corresponding E_{ads} using the distorted surface (higher energy) as reference are presented in bold and linked with arrows below (a) and (b). The interface structures are represented following the same colour code as the previous figures.

on the etched $TiO_{1.75}$-TiN interface induces a migration along the normal of the Ti that binds with the adsorbed O of 0.48 Å for the molecular adsorption mode, 1.02 Å for the dissociated model and 0.17 Å after desorption, estimated with respect to the initial position of Ti on the pristine surface. The distances of the Ti-O bonds formed on the surface are 2.11 Å for H_2O and 1.91 Å for OH.

On the $TiO_{1.75}$-TiN interface generated from the 2-layer **slab model** (Figure 8), H_2O is adsorbed on the surface forming a Ti-O bond with length 2.20 Å which is shortened to 1.89 Å after dissociation. If we use again the distorted surface as reference, that has higher energy than the initially bare surface, the computed adsorption energy for an H_2O molecule is -1.28 eV and it is more stable than the model containing dissociated water (E_{ads} = -0.87 eV). In addition, an extra Ti^{3+} cation is present in the oxide as a result of electronic relocalisation after water adsorption/desorption process. We can thus conclude that, except for the 2-layer thick **slab model** interface, which exhibit a strongly distorted surface, all the models for the adsorption of isolated water on TiO_2-TiN interfaces show that dissociated water is more stable than molecular adsorption. These differences range from 0.41 eV to 0.94 eV. Our findings are in line with previous theoretical studies of water adsorption on rutile (110) or and 4-layer thick TiO_2-TiN interfaces, where the preference for dissociative adsorption for single isolated water molecules at rutile (110) was shown. Our computed energy differences are larger than the 0.11 eV estimated for water dissociation on rutile (110)[55] or 0.34 eV on 4-layer thick TiO_2-TiN interface.[54] The present results also show that the adsorption energy of an isolated OH-H is stronger at the 1-layer thick stoichiometric TiO_2-TiN interface compared to the thicker oxides or non-stoichiometric models. This is a consequence of the large concentration of reduced Ti^{3+} that arise on surface sites when a very thin TiO_2 forms an interface with TiN in combination with the non-ordered structure that contributes towards the further stabilization of this ultra-thin oxide layer.

3.3.2 Adsorption of water at higher coverages

At the highest water coverage, the fully covered 1-layer model (Figure 9) has six H_2O molecules deposited on the available Ti under-coordinated sites on the surface. The relaxed structures for the models with molecular and dissociated water are presented in Figure 9(a) and Figure 9(b) respectively. Both models are almost degenerate in energy, with computed adsorption energies per water molecule of -0.81 eV for molecular H_2O and -0.84 eV for OH-H. Closer inspection shows that upon relaxation, 3 water molecules form when starting from the initially fully hydroxylated surface (these are indicated with dashed rings in Figure 9(b)) leading to a mixed environment in which molecular H_2O and hydroxyls coexist. On the molecular H_2O covered surface, five of the H_2O bind to surface Ti with bond distances between 2.22-2.33 Å while one of the molecules interacts with surface O on the surface through a hydrogen bond with an O---H distance of 2.06 Å.

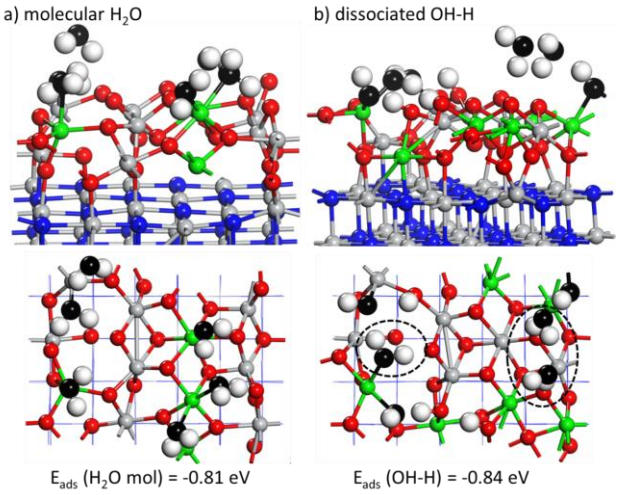

Figure 9. Structure fully covered 1-layer thick TiO_2 -TiN interface with (a) molecular water and (b) dissociated water adsorption modes. The adsorption energy values per adsorbed water are presented under figures. Molecular H_2O formed from OH+H reassociation are indicated with dashed rings. The Ti^{3+} atoms in TiO_2 are represented by green spheres, Ti^{4+} atoms in TiO_2 and all Ti in TiN are grey, N atoms are blue, O atoms from TiO_2 are red, O atoms from adsorbed water are black and H atoms are white.

The bonds created between surface Ti and O from H_2O are shorter on the hydroxylated surface. The three OH and the closest H_2O to the surface bind with Ti-O distances between 1.97-2.17 Å. The two remaining water molecules sit further from the surface at distances of 2.77 Å and 2.83 Å from the nearest surface Ti and bind to surface O with Hydrogen-bonds that have O---H distances of 1.88 Å and 1.84 Å. The two adjacent H_2O molecules, at

a distance of 1.94 Å, also interact through non-bonding O-H interactions. These results indicate that when a very thin oxide layer is deposited on TiN, forming a nearly amorphous or nanostructured oxide, molecular water may coexist along with hydroxyls when water pressures are equal or higher than regular ambient conditions.

Moving now to the 2 layer oxide models, molecular water adsorption at full coverage is the most stable on the perfect interface (Figure 10). On the surface, the two rows with 3 H_2O molecules each align on the rutile surface along the [1$\bar{1}$0] direction via formation of strong H-bonds between adjacent water molecules, stabilizing the fully covered model. The preference for the aligned distribution is in agreement with previous studies on water adsorption at TiO_2 rutile (110)[55,77] and 4-layer thick TiO_2-TiN interfaces.[54] On the model with all water molecules dissociated, hydroxyls on the surface go through a barrierless reaction to reassociate and form water molecules (Figure S3), which indicates the instability of dissociated water on fully covered ordered rutile (110) surfaces.

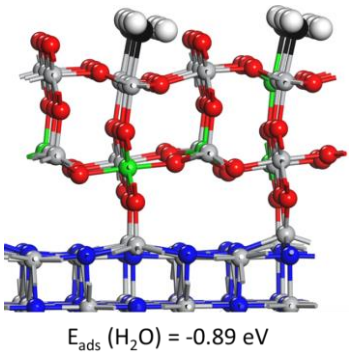

Figure 10. Structure of a water monolayer (1ML) on perfect 2-layer thick rutile (110) TiO_2 -TiN interface. The adsorption energy per adsorbed water is presented under the figure. The Ti^{3+} atoms in TiO_2 are represented by green spheres, Ti^{4+} atoms in TiO_2 and all Ti in TiN are grey, N atoms are blue, O atoms from TiO_2 are red, O atoms from adsorbed water are black and H atoms are white.

The 2-layer thick non-stoichiometric $TiO_{1.75}$-TiN models allow accommodating up to five H_2O binding directly to surface Ti through the formation of Ti-O bonds. The interfacial and surface relaxations upon vacancy formation leads to the presence of Ti_{5f} sites on the surface that are available for water adsorption, instead of the six available sites on the rutile (110) stoichiometric model. Water adsorbs strongly on the etched $TiO_{1.75}$-TiN interface (Figure 11), due to the contribution of surface relaxations to the overall decreasing of the total energy. The molecular adsorption of E_{ads} = -1.73 eV per water is very similar to the energy of the dissociative adsorption mode with E_{ads} = -1.66 eV.

The two models display a mixed H_2O and OH coverage on the surface. From a 1 ML coverage of molecular water, one water molecule adsorbs dissociatively upon relaxation, Figure 11(a). On the surface with 1 ML coverage of water in dissociated mode, one water molecule forms upon relaxation, Figure 11(b). The bonds formed between surface Ti and the adsorbed O are consistently larger for molecular H_2O with measured distances in a range between 2.20-2.27 Å from O in H_2O and 2.12 Å from O in OH. The bond distances on the hydroxylated layer vary between 1.88 - 2.01 Å from OH and 2.22 Å from H_2O.

The small difference in energy between models along with the coexistence of H_2O and surface OH suggest the likely stability of mixed layer of hydroxyls along with water molecules at high water coverages on non-stoichiometric and distorted rutile (110) interfaces, where the formation of stable H_2O islands may take place.

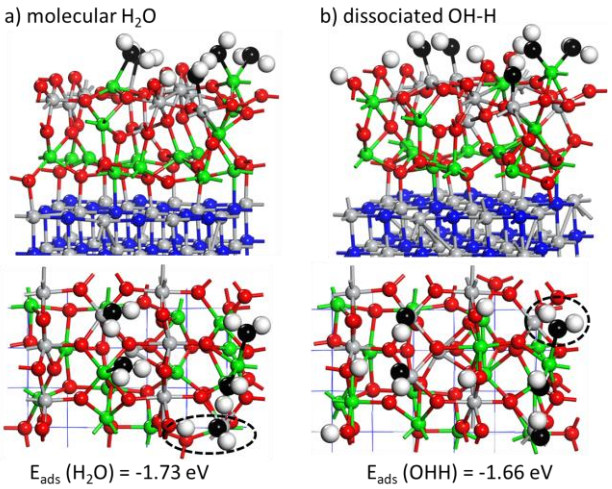

Figure 11. Structures of fully covered 2-layer thick **etched model** of TiO_2 -TiN interfaces with (a) molecular water and (b) dissociated adsorption modes. The adsorption energy values per adsorbed water are presented under figures. The Ti^{3+} atoms in TiO_2 are represented by green spheres, Ti^{4+} atoms in TiO_2 and all Ti in TiN are grey, N atoms are blue, O atoms from

TiO_2 are red, O atoms from adsorbed water are black and H atoms are white.

The adsorption of water on the 2-layer thick non-ordered **slab model** TiO_2-TiN interface, depicted in Figure 12, leads to a more moderated decrease of the total energy compared to the etched interface, as a consequence of the higher stability of this interface. The fully covered hydroxylated surface (E_{ads} = -0.71 eV per water molecule) is more stable than the H_2O covered model (E_{ads} = -0.55 eV per water molecule). In the latter, one of the H_2O molecules spontaneously dissociates upon relaxation to form an OH-H pair on the surface. The bonds formed between surface Ti and the adsorbed O are again larger for molecular H_2O.

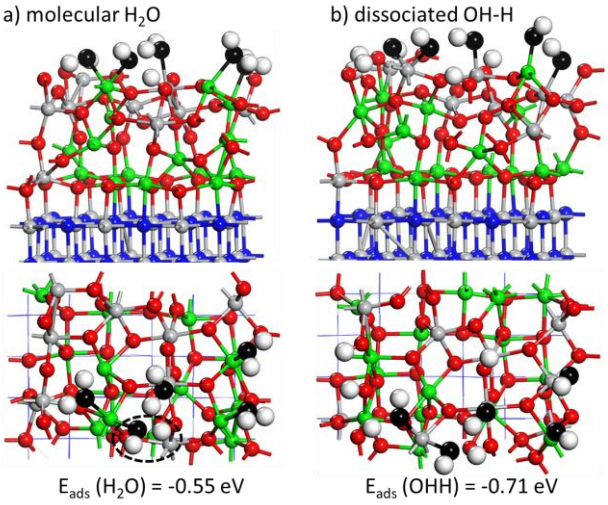

Figure 12. Structures of fully covered 2-layer thick **slab model** of TiO_2 -TiN interfaces with (a) molecular water and (b) dissociated adsorption modes. The adsorption energy values per adsorbed water are presented under figures. Molecular H_2O that dissociates spontaneously to form OH+H is indicated with a dashed ring. The Ti^{3+} atoms in TiO_2 are represented by green spheres, Ti^{4+} atoms in TiO_2 and all Ti in TiN are grey, N atoms are blue, O atoms from TiO_2 are red, O atoms from adsorbed water are black and H atoms are white.

The Ti-O distances on the molecular model (Figure 12(a)) range between 2.20 - 2.27 Å as measured from O in H_2O and 2.12 Å from O in the single OH on the surface. Bond distances on the hydroxylated layer (Figure 12(b)) range between 1.85 - 1.97 Å as measured from the adsorbed O in the OH termination. The energy difference of 0.16 eV per water with the barrierless dissociation of water on the H_2O covered surface suggest the preferential stability of hydroxyls against molecular water on a highly non-stoichiometric oxide that presents a disordered structure and with a large concentration of reduced Ti^{3+} cations. The preferential formation of hydroxyls as a result of the high concentration of reduced Ti^{3+} in TiO_2 induced by UV illumination has been experimentally observed and it is also proposed to increase the hydrophilicity of the surface.[18] Our models show the formation of stable hydroxyls on highly non-stoichiometric TiO_{2-x} surfaces, which contain larger proportions of Ti^{3+} cations than the stoichiometric interfaces and lacks the high order of a crystalline surface layer that permits molecular H_2O to form stable rows or islands on the oxide surface.

3.4. Thermodynamics of water adsorption at TiO_2-TiN

In this section, we analyze the relative stability of the interfaces when they are in thermodynamic equilibrium with the environment. We use the results at 0K obtained by DFT calculations and include the effect of oxygen and water present in the atmosphere. We model the system as it exchanges particles with an external reservoir, which is imagined to be infinitely large so that the chemical potentials of the species do not change during the process. In the previous section, we calculated the oxygen vacancy formation energies for single and double TiO_2 layer on TiN, and we deduced that the formation of a single vacancy is favourable compared to the multiple vacancies in the 1-layer slab while in the 2-layer model the opposite trend is observed. These results are in line with our *ab initio* thermodynamics analysis, which shows that the inclusion of realistic environmental variable indicates that multiple vacancies are most stable at low (reducing) oxygen chemical potential values.

As shown in Fig.13, in the interface formed by a single TiO_2 layer, the single vacancy is the most stable for a large very range of $\Delta\mu_0$, and the highly reduced interface becomes stable only if $\Delta\mu_0$ is lower than -3.0 eV. On the other hand, when a double layer of TiO_2 is deposited on TiN, we have two possible distinct scenarios for the formation of a single O vacancy: at the TiO_2 surface or at the TiO_2-TiN interface. In both cases, the pristine interface is stable at low $\Delta\mu_0$, whereas decreasing $\Delta\mu_0$ the multiple interfacial vacancy system

becomes stable. However, the ideal interface shows temperature/pressure "resistance" to reduction if compared to the non-stoichiometric oxide slabs.

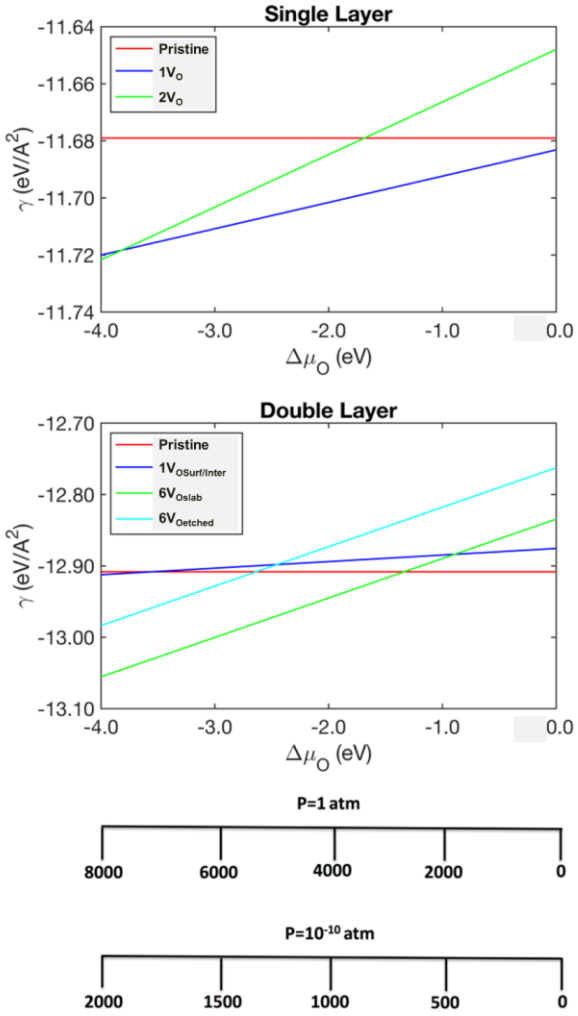

Figure 13. Interface energy (γ) as a function of the chemical potential of oxygen ($\Delta\mu_0$) as defined in the methodology section. Top and bottom plots represent respectively the interface formed by TiN and a TiO_2 single and double layer. The negative values of $\Delta\mu 0$ correspond to reducing atmospheric conditions. The red and blue lines represent the interface energy of pristine model and with one oxygen vacancy in the single layer ($1V_O$) and double layer ($1V_{OSurf/Inter}$) models, where the systems with surface and interfacial O vacancy are represented together. The green and cyan represent the interface in highly reduced conditions, that is with two oxygen vacancies for TiO_2 single layer ($2V_O$), and six oxygen vacancies for TiO_2 double layer in the slab ($6V_{Oslab}$) and etched ($6V_{Oslab}$) models. We include two additional scales that represent the conversion in temperature (K) of the chemical potential of the oxygen, calculated to p=1atm and $p=10^{-10}$atm

When taking into account the effect of the water, we have to include in the model an additional reservoir that is in equilibrium with the interface. However, in our model, the two reservoirs are in non-equilibrium with each other, so that we are able to treat the two variable μ_0 and μ_{H2O} independently and consequently explore a wider range of possible conditions. In Fig.14 we show the chemical potential of water from 0 to -3.0 eV, however, to consider water vapour as a thermodynamically stable phase, the maximum value that $\Delta\mu_{H2O}$ can assume is −0.91 eV, which corresponds to the chemical potential of water at the experimental critical point.

As a first analysis, we compare the relative stability of the interface formed by a single TiO_2 layer on TiN. Here, we consider a "dry" interface model with the single oxygen vacancy and highly reduced with the multiple oxygen vacancies. Additionally, we consider the single oxygen vacancy and pristine interfaces with low and high water coverages of water. At regular ambient pressure, the pristine interface model fully covered with a mixture of molecular and dissociated water (Figure 9(b)) appears as the most stable configuration. At higher temperatures, the model with isolated water adsorbed in dissociated mode (Figure 5(b)) is stabilized at P_{O2} and P_{H2O} of 1 atm. We notice that the pristine interface is not stable under any conditions, and the highly reduced interface becomes stable only at very low values of both water and oxygen chemical potentials.

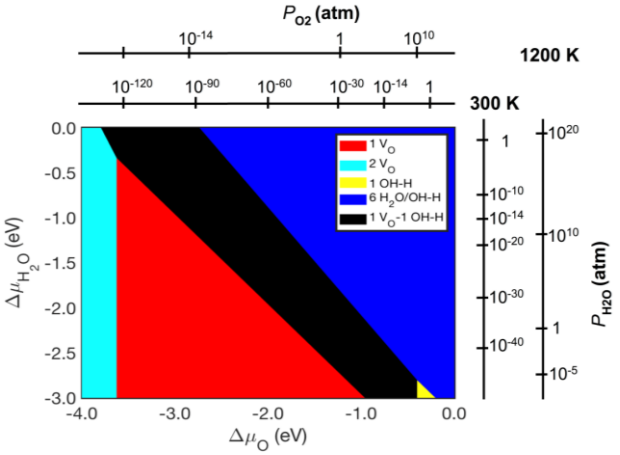

Figure 14. Interface energy (γ) as a function of the chemical potential of oxygen ($\Delta\mu_O$) and water ($\Delta\mu_{H2O}$) as defined in the methodology section. Top and bottom plots represent respectively the interface formed by TiN and a TiO_2 single layer. Here, the pristine surface is taken into account together

with the low and highly reduced "dry" interfaces, and the low reduced and pristine interfaces in low and high water adsorbed concentration. The coloured areas represent the conditions where each interface is thermodynamically stable with respect to the other interface considered. Here OH-H indicates dissociated adsorption of water. We include two additional scales for each axis that represent the conversion in pressure (atm) of the chemical potential of the oxygen, calculated at T=300K and T=1200K.

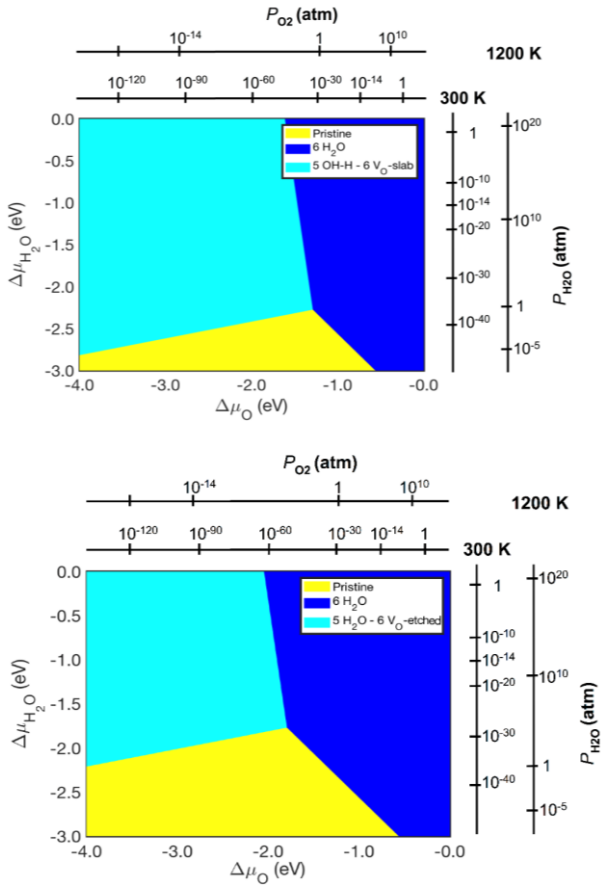

Figure 15. Interface energy (γ) as a function of the chemical potential of oxygen ($\Delta\mu_O$) and water ($\Delta\mu_{H2O}$) as defined in the methodology section. Top and bottom plots represent respectively the interface formed by TiN and a TiO_2 double layer in **slab** and **etched** configuration. Here, the pristine surface is taken into account together with the low and highly reduced "dry" interfaces, and the low reduced and pristine interfaces in low and high water adsorbed concentration. The coloured areas represent the conditions where each interface is thermodynamically stable with respect to the other interface considered. Here, H_2O and OH-H indicate molecular and dissociated adsorption, respectively. We include two additional scales for each axis that represent the conversion in pressure (atm) of the chemical potential of the oxygen, calculated at T=300K and T=1200K.

When considering the 2-layer TiO_2 either in **etched** or **slab** configuration, the analysis leads to a different conclusion. In this case, only three surfaces are stable within the considered range: pristine, highly hydrated and highly hydrated/highly reduced surfaces. The fully water covered stoichiometric models appear as the most stable structure at room temperature and pressure conditions. As discussed in the previous sections, our study considers the formation of O vacancies starting from a perfect interface. However, defects are prone to form and remain trapped during oxide growth, and thus, non-stoichiometric oxide slabs can be stabilized at ambient conditions. The major difference between etched and slab configuration is that in etched conditions the highly hydrated interface is stable for a larger range of both $\Delta\mu_O$ and $\Delta\mu_{H2O}$.

3.5. Electronic structure of bare and hydrated TiO_2-TiN interface models

In this section, we discuss the electronic features of the different TiO_2-TiN interfaces and how these are affected by the adsorption of water. The electronic density of states (EDOS) for the 1-layer (stoichiometric) and 2-layer (stoichiometric and O-defective) TiO_2-TiN interfaces are presented in Figure 16 and Figure 17 respectively. The individual contribution of each element projected onto Ti 3d, N 2p and O 2p states are represented in different panels for the TiN and TiO_2 regions. A more detailed representation of the EDOS for all the bare and hydrated interfacial models in this study are included in the supporting information (Figures S6-9), whereas the most important features for selected cases are discussed below.

The distribution of the TiN EDOS represents the metallic character of this material due to the main contribution of Ti d-electrons to the states near the Fermi level (E_F). The EDOS shows Ti-N hybridization in for the states below -2 eV with a main peak centred at -5 eV, measured both with respect to E_F. These features are common to all the interfaces and do not seem to be strongly affected by the thickness of the oxide or presence of defects in the oxide or the adsorption of water. Therefore, we will omit the description of the TiN in the successive discussion.

The TiO_2 EDOS shows the semiconductor character of this metal-oxide. The O 2p states

dominate the states under the top edge of the valence band (VBM) with some Ti 3d contribution while the Ti 3d are the main responsible for the states at the bottom of the conduction band (CBM). We measured an energy gap between the valence and conduction bands of 2.7 eV in the 1-layer oxide slab and 2.6 eV for the 2-layer. These values are comparable to the main gap of the 4-layer thick oxide in a TiO_2-TiN interface of 2.5 eV,[40] calculated with an identical computational setup, and underestimated compared to the experimental value of TiO_2 gap of around 3 eV.[78] The underestimated values for the energy gap are generally observed in DFT and DFT+U simulations of rutile TiO_2 and do not affect the results presented in this work. The Ti^{3+} states lay between the highest

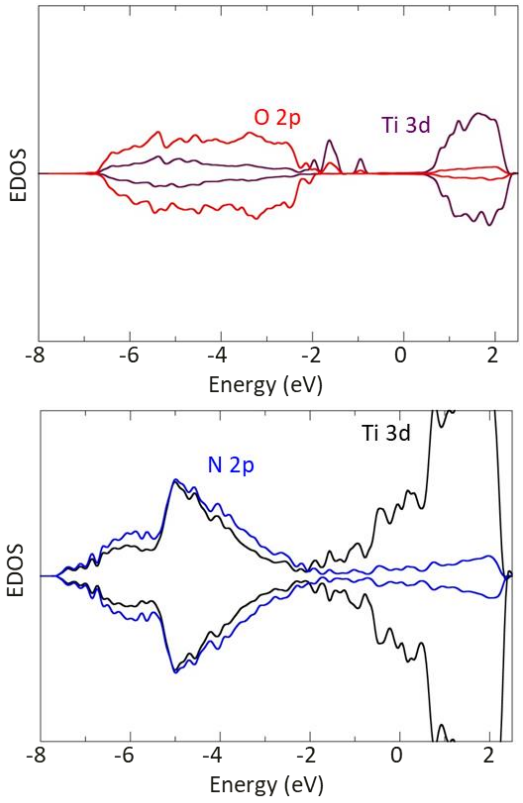

Figure 16. Spin-polarized electronic Density of States (EDOS) of 1-layer thick stoichiometric TiO_2-TiN interface. The graphs on the top and bottom panels represent TiO_2 and TiN EDOS. A legend with the contribution of each species is included in the graphs. Ti 3d electrons from TiN are represented with black lines, N 2p electrons in blue, Ti 3d electrons from TiO_2 in purple, and O 2p electrons from TiO_2 in red. The accumulated contribution of each species was considered for the total EDOS. The upper and lower halves of the graphs represent the spin-up and spin-down components respectively. The 0 eV energy stands for the Fermi level.

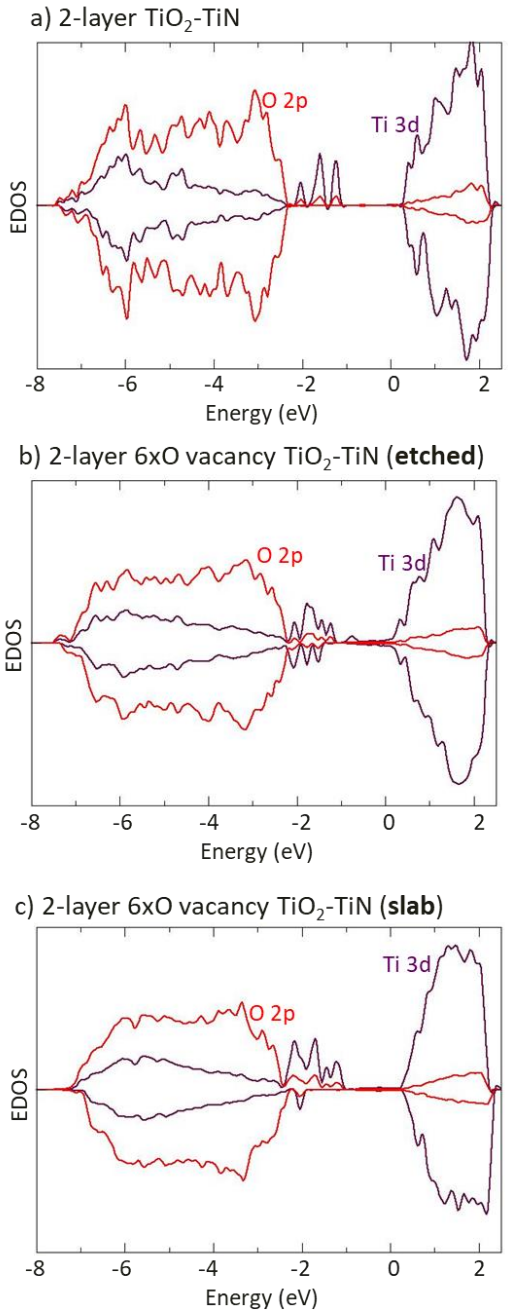

Figure 17. Spin-polarized electronic Density of States (EDOS) of 2-layer thick TiO_2-TiN interfaces (a) stoichiometric, (b) **etched** model of $Ti_{1.75}$-TiN and (c) **slab** model of $Ti_{1.75}$-TiN.

occupied states O 2p states and the lowest unoccupied Ti 3d states in TiO_2 as is commonly observed in reduced TiO_2[73] and other Ti-based metal-oxide interfacial systems like NiTi-TiO_2.[79] In the 1-layer model (Figure 16), the reduced Ti^{3+} states occupy the states between VBM and -1.4 eV below E_F, which potentially reduces the energy gap

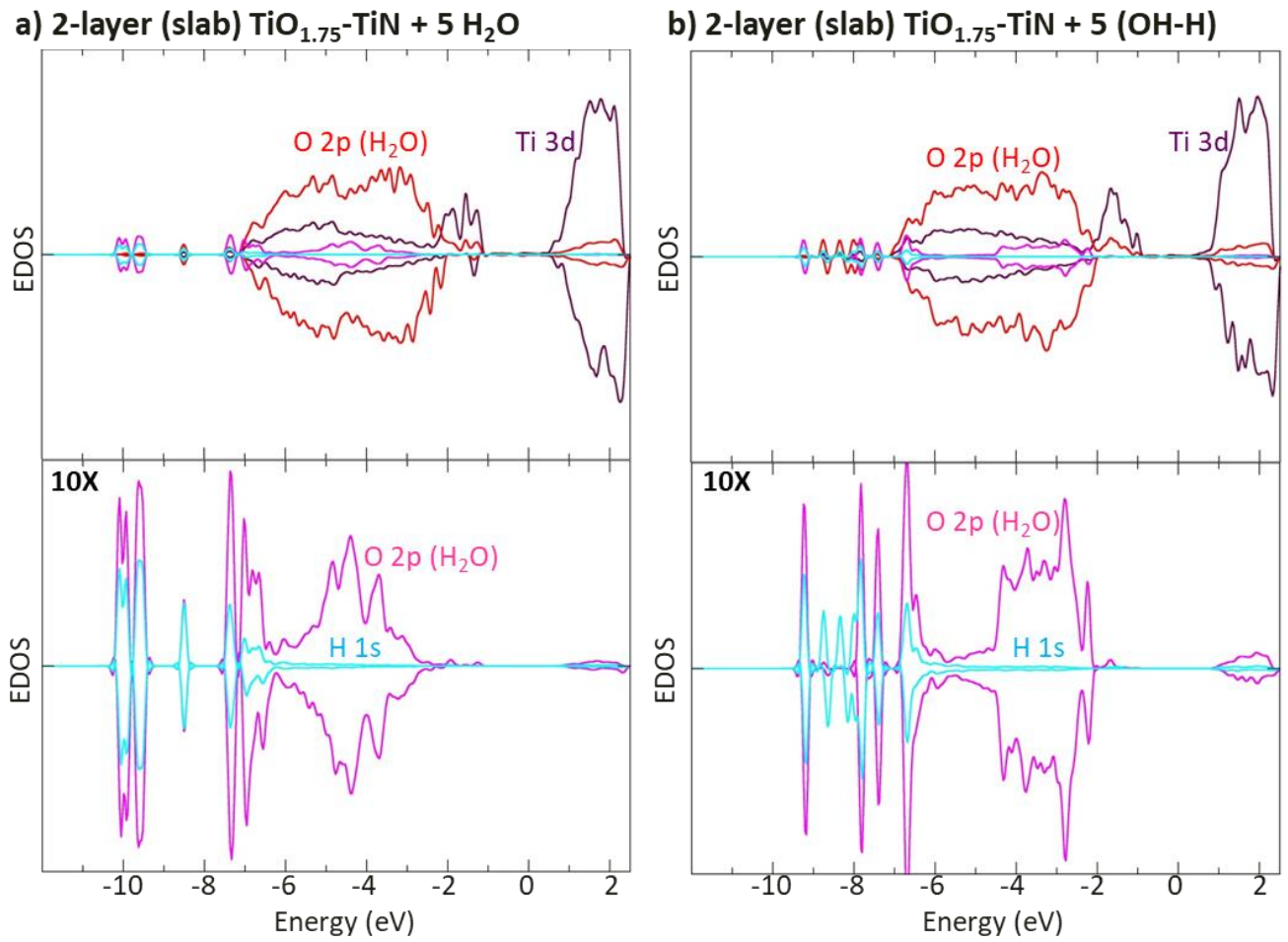

Figure 18. Spin-polarized Electronic Density of States (EDOS) of TiO_2 for the fully covered **slab model** of $Ti_{1.75}$-TiN with (a) molecular H_2O and (b) dissociated OH-H water. A legend with the contribution of each species is included in the graphs. Ti 3d electrons from TiN are represented with black lines, N 2p electrons in blue, Ti 3d electrons from TiO_2 in purple and O 2p electrons from TiO_2 in red. The accumulated contribution of each species was considered for the total EDOS. The upper and lower halves of the graphs represent the spin-up and spin-down components, respectively. The 0 eV energy stands for the Fermi level.

to 1.9 eV. We observe also a small peak located in the mid-gap and centred at -1 eV from E_F. The formation of one oxygen vacancy in the 1-layer system does not produce significant changes in the partial EDOS, as can be observed in Figure S4.

The stoichiometric 2-layer oxide slab (Figure 17.a) exhibits an electronic energy gap of 2.6 eV with a mid-gap contribution from reduced Ti^{3+} states lying between 0.5 eV above VBM and 1.3 eV below CBM. In the non-stoichiometric slabs, with $TiO_{1.75}$ composition, the Ti^{3+} states occupy the states from VBM to about -1 eV below E_F. The presence of the Ti^{3+} states contributes to a significant reduction of the energy gap, from 2.6 eV in the stoichiometric TiO_2-TiN model to 1.3 eV in the $TiO_{1.75}$-TiN systems.

The adsorption of water on the oxide slabs in TiO_2-TiN interfaces, presented in Figure 18 and Figures S7-S9, does not produce significant alterations in the TiO_2 EDOS. The EDOS for the 2-layer thick O-defective fully covered $TiO_{1.75}$-TiN interfaces model exhibit equivalent features for the etched and slab model interfaces. However, we observe clear differences in the EDOS between molecular and dissociative adsorption of water. In the interface with adsorbed H_2O (Figure 18.a) the main O 2p states from H_2O are distributed between -1.4 eV and -3.0 eV below the TiO_2 valence band, with several sharp O and H peaks in the region between

-4.2 eV and -8.1 eV as measured from VBM. When water is dissociatively adsorbed, the hybridization between O 2p states from TiO_2 and OH is identified at higher energy states, with their main contribution between -0.6 eV and -2.4 eV below VBM. The O and H states from dissociated water are localized in a region between -4.9 eV and -7.9 eV below VBM. The most strongly bonded states (lowest energy) are more stable in the hydroxylated model compared to the model with molecular H_2O. The presence of several sharp peaks, that are localized at low energy states, denote the high stability of the adsorbed hydroxyls on the non-stoichiometric non-ordered $TiO_{1.75}$-TiN interface. In addition, the high concentration of reduced Ti^{3+} states formed from charge transfer from the TiN substrate along with the formation of stable O vacancies leads to a significant reduction of the energy gap of this system compared to the stoichiometric slab, as discussed above.

4. CONCLUSIONS

We carried out a detailed first-principles study to describe the structural and electronic properties of ultra-thin TiO_2 supported on a rock-salt TiN surface model. The rutile (110) TiO_2 slab models are stabilized on the TiN surface through the formation of interfacial Ti – O bonds. Our Hubbard-corrected DFT+U calculations show charge transfer from the TiN towards the oxide, which leads to the formation of reduced Ti^{3+} cations in TiO_2. The 1-layer model presents a strongly distorted oxide, due to the high concentration of reduced Ti^{3+} atoms and the compression applied to TiO_2 to compensate the lattice mismatch with TiN. Our ab initio thermodynamics calculations show the stability of oxygen vacancies in this interface for values of $\Delta\mu_0$ below -1.25 eV.

The oxide slab in the 2-layer thick TiO_2-TiN interfaces preserves the original symmetry of the rutile surface. The highly non-stoichiometric ($TiO_{1.75}$-TiN interface) **slab model**, generated by introducing six interfacial O vacancies in the 2-layer thick perfect interface, is highly distorted and it is more stable than the **etched oxide model**. The introduction of several vacancies in an already non-stoichiometric system becomes progressively more favourable, which suggests the stability of the highly non-stoichiometric interfaces, in line with our previous study on nitride supported interfaces with thicker oxide. [40]

We analysed the adsorption of molecular and dissociated water as a function of the surface coverage and the composition of the oxide-nitride interface. One isolated water is dissociatively adsorbed on the stoichiometric and at the least distorted O-vacancy oxide slabs. At higher water coverages, our results suggest the likely stability of mixed environments with molecular H_2O and hydroxyls on the 1-layer slab. On the 2-layer TiO_2 slab, 1ML of molecular H_2O coverage is stabilized through the formation of H-bonds between adjacent water molecules. On the other hand, the adsorption of a 1ML on the 2-layer thick non-ordered **slab model** presents the hydroxylated surface (E_{ads} = -0.71 eV per H_2O) as the most energetically favoured model. This is mainly due to the lack of symmetry on the oxide surface, that penalises the stabilization of H_2O avoiding the formation of H bonds with its neighbouring molecules.

The EDOS for the highly non-stoichiometric $TiO_{1.75}$-TiN systems shows the Ti^{3+} states lying above the top of the valence band, which contributes to a significant reduction of the energy gap, from 2.6 eV in the stoichiometric TiO_2-TiN model to 1.3 eV in $TiO_{1.75}$-TiN.

Our DFT+U study of ultrathin oxide in TiO_2–TiN interfaces indicate the preference for dissociated water on the amorphous-like oxide slabs along with an important reduction of the electronic energy gap in the interfaces with highly non-stoichiometric oxides. Based on these analyses, we suggest the suitability of this interfacial system for photocatalytic water splitting applications. The main outcomes of this study can be also used as a guide to foster future applications for interfaces with ultra-thin oxide supported on a metallic substrate.

REFERENCES

1 Zhang, S. & Zhu, W. TiN coating of tool steels: a review. *Journal of Materials Processing Technology* **39**, 165-177 (1993).

2 Van Hove, R. P., Sierevelt, I. N., van Royen, B. J. & Nolte, P. A. Titanium-

nitride coating of orthopaedic implants: a review of the literature. *BioMed Research International* **2015**, 485975/485971-485975/485979, doi:10.1155/2015/485975 (2015).

3 Toth, L. *Transition metal carbides and nitrides*. (Academic Press, 1971).

4 Pierson, H. O. *Handbook of Refractory Carbides & Nitrides: Properties, Characteristics, Processing and Apps*. (William Andrew, 1996).

5 Vaz, F. *et al.* Mechanical characterization of reactively magnetron-sputtered TiN films. *Surface and Coatings Technology* **174**, 375-382 (2003).

6 Johansson, L. I. Electronic and structural properties of transition-metal carbide and nitride surfaces. *Surface Science Reports* **21**, 177-250 (1995).

7 Patsalas, P., Kalfagiannis, N. & Kassavetis, S. Optical properties and plasmonic performance of titanium nitride. *Materials* **8**, 3128-3154 (2015).

8 Nakayama, T., Wake, H., Ozawa, K., Nakamura, N. & Matsunaga, T. Electrochemical prevention of marine biofouling on a novel titanium-nitride-coated plate formed by radio-frequency arc spraying. *Applied Microbiology and Biotechnology* **50**, 502-508, doi:10.1007/s002530051327 (1998).

9 Nakayama, T. *et al.* Use of a titanium nitride for electrochemical inactivation of marine bacteria. *Environmental Science & Technology* **32**, 798-801 (1998).

10 Patsalas, P. *et al.* Conductive nitrides: Growth principles, optical and electronic properties, and their perspectives in photonics and plasmonics. *Materials Science and Engineering: R: Reports* **123**, 1-55 (2018).

11 Kelly, P. J. & Arnell, R. D. Magnetron sputtering: a review of recent developments and applications. *Vacuum* **56**, 159-172 (2000).

12 Abadias, G., Tse, Y., Guérin, P. & Pelosin, V. Interdependence between stress, preferred orientation, and surface morphology of nanocrystalline TiN thin films deposited by dual ion beam sputtering. *Journal of Applied Physics* **99**, 113519 (2006).

13 Cheng, Y., Tay, B., Lau, S., Kupfer, H. & Richter, F. Substrate bias dependence of Raman spectra for TiN films deposited by filtered cathodic vacuum arc. *Journal of Applied Physics* **92**, 1845-1849 (2002).

14 Abadias, G. Stress and preferred orientation in nitride-based PVD coatings. *Surface and Coatings Technology* **202**, 2223-2235 (2008).

15 Jindal, P., Santhanam, A., Schleinkofer, U. & Shuster, A. Performance of PVD TiN, TiCN, and TiAlN coated cemented carbide tools in turning. *International Journal of Refractory Metals and Hard Materials* **17**, 163-170 (1999).

16 Nordin, M., Larsson, M. & Hogmark, S. Mechanical and tribological properties of multilayered PVD TiN/CrN, TiN/MoN, TiN/NbN and TiN/TaN coatings on cemented carbide. *Surface and Coatings Technology* **106**, 234-241 (1998).

17 Wagner, J. *et al.* The effect of deposition temperature on microstructure and properties of thermal CVD TiN coatings. *International Journal of Refractory Metals and Hard Materials* **26**, 120-126 (2008).

18 Lee, H. Y., Park, Y. H. & Ko, K. H. Correlation between surface morphology and hydrophilic/hydrophobic conversion of MOCVD− TiO_2 films. *Langmuir* **16**, 7289-7293 (2000).

19 Rebenne, H. E. & Bhat, D. G. Review of CVD TiN coatings for wear-resistant applications: deposition processes, properties and performance. *Surface and Coatings Technology* **63**, 1-13 (1994).

20 Elers, K.-E., Winkler, J., Weeks, K. & Marcus, S. $TiCl_4$ as a precursor in the TiN deposition by ALD and PEALD. *Journal of the Electrochemical society* **152**, G589-G593 (2005).

21 Westlinder, J. *et al.* On the thermal stability of atomic layer deposited TiN as gate electrode in MOS devices. *IEEE Electron Device Letters* **24**, 550-552 (2003).

22 Ernsberger, C., Nickerson, J., Smith, T., Miller, A. & Banks, D. Low temperature oxidation behavior of reactively sputtered TiN by X- ray photoelectron spectroscopy

and contact resistance measurements. *Journal of Vacuum Science & Technology A: Vacuum, Surfaces, and Films* **4**, 2784-2788 (1986).

23 Hou, X., Chou, K. C. & Zhang, M. The model for oxidation kinetics of titanium nitride coatings. *International Journal of Applied Ceramic Technology* **7**, 248-255 (2010).

24 Wittmer, M., Noser, J. & Melchior, H. Oxidation kinetics of TiN thin films. *Journal of Applied Physics* **52**, 6659-6664 (1981).

25 Rebouta, L., Vaz, F., Andritschky, M. & da Silva, M. F. Oxidation resistance of (Ti,Al,Zr,Si)N coatings in air. *Surface and Coatings Technology* **76**, 70-74 (1995).

26 Suni, I., Sigurd, D., Ho, K. & Nicolet, M. A. Thermal oxidation of reactively sputtered titanium nitride and hafnium nitride films. *Journal of the Electrochemical Society* **130**, 1210-1214 (1983).

27 Desmaison, J., Lefort, P. & Billy, M. Oxidation mechanism of titanium nitride in oxygen. *Oxidation of Metals* **13**, 505-517 (1979).

28 Uetani, K. *et al.* Oxidation mechanism of ultra thin TiN films prepared by an advanced ion-plating method. *Materials Transactions* **42**, 403-406 (2001).

29 Gwo, S. *et al.* Local electric-field-induced oxidation of titanium nitride films. *Applied Physics Letters* **74**, 1090-1092 (1999).

30 Kawasaki, H. *et al.* TiO_2/TiN/TiO_2 heat mirrors by laser ablation of single TiN target. *Journal of Physics: Conference Series* **100**, 012038 (2008).

31 Jung, M. J. *et al.* High-rate and low-temperature synthesis of TiO_2, TiN, and TiO_2/TiN/TiO_2 thin films and study of their optical and interfacial characteristics. *Journal of Vacuum Science & Technology B: Microelectronics and Nanometer Structures Processing, Measurement, and Phenomena* **23**, 1826-1831, doi:10.1116/1.1978903 (2005).

32 Qamar, S. *et al.* Ultrathin TiO_2 flakes optimizing solar light driven CO_2 reduction. *Nano Energy* **26**, 692-698 (2016).

33 Zhao, Y. *et al.* Tuning Oxygen Vacancies in Ultrathin TiO_2 Nanosheets to Boost Photocatalytic Nitrogen Fixation up to 700 nm. *Advanced Materials*, 1806482 (2019).

34 Xie, Z., Liu, X., Zhan, P., Wang, W. & Zhang, Z. Tuning the optical bandgap of TiO2-TiN composite films as photocatalyst in the visible light. *AIP Advances* **3**, 062129, doi:10.1063/1.4812702 (2013).

35 Morikawa, T., Asahi, R., Ohwaki, T., Aoki, K. & Taga, Y. Band-gap narrowing of titanium dioxide by nitrogen doping. *Japanese Journal of Applied Physics* **40**, L561 (2001).

36 Di Valentin, C. *et al.* N-doped TiO_2: theory and experiment. *Chemical Physics* **339**, 44-56 (2007).

37 Zimmermann, J., Finnis, M. W. & Ciacchi, L. C. Vacancy segregation in the initial oxidation stages of the TiN(100) surface. *The Journal of Chemical Physics* **130**, 134714/134711-134714/134711, doi:10.1063/1.3105992 (2009).

38 Hegde, R. I., Fiordalice, R. W., Travis, E. O. & Tobin, P. J. Thin film properties of low- pressure chemical vapor deposition TiN barrier for ultra- large- scale integration applications. *Journal of Vacuum Science & Technology B* **11**, 1287-1296 (1993).

39 Moatti, A., Bayati, R. & Narayan, J. Epitaxial growth of rutile TiO_2 thin films by oxidation of TiN/Si{100} heterostructure. *Acta Materialia* **103**, 502-511, doi:10.1016/j.actamat.2015.10.022 (2016).

40 Gutiérrez Moreno, J. J. & Nolan, M. Ab initio study of the atomic level structure of the rutile TiO_2(110)–titanium nitride (TiN) interface. *ACS Applied Materials & Interfaces* **9**, 38089-38100, doi:10.1021/acsami.7b08840 (2017).

41 Diebold, U. The surface science of titanium dioxide. *Surface Science Reports* **48**, 53-229 (2003).

42 Bao, S. J. *et al.* New nanostructured TiO_2 for direct electrochemistry and glucose sensor applications. *Advanced Functional Materials* **18**, 591-599 (2008).

43 Lin, H.-M., Keng, C.-H. & Tung, C.-Y. Gas-sensing properties of nanocrystalline

TiO_2. *Nanostructured Materials* **9**, 747-750 (1997).

44 Pan, J., Leygraf, C., Thierry, D. & Ektessabi, A. Corrosion resistance for biomaterial applications of TiO_2 films deposited on titanium and stainless steel by ion- beam- assisted sputtering. *Journal of Biomedical Materials Research Part A* **35**, 309-318 (1997).

45 Hashimoto, K., Irie, H. & Fujishima, A. TiO_2 photocatalysis: a historical overview and future prospects. *Japanese Journal of Applied Physics* **44**, 8269 (2005).

46 Geetha, M., Singh, A., Asokamani, R. & Gogia, A. Ti based biomaterials, the ultimate choice for orthopaedic implants–a review. *Progress in Materials Science* **54**, 397-425 (2009).

47 Graziani, L., Quagliarini, E., Bondioli, F. & D'Orazio, M. Durability of self-cleaning TiO_2 coatings on fired clay brick façades: Effects of UV exposure and wet & dry cycles. *Building and Environment* **71**, 193-203 (2014).

48 Lorenzetti, M. *et al.* Surface properties of nanocrystalline TiO_2 coatings in relation to the in vitro plasma protein adsorption. *Biomedical Materials* **10**, 045012, doi:10.1088/1748-6041/10/4/045012 (2015).

49 Wang, R. *et al.* Photogeneration of highly amphiphilic TiO_2 surfaces. *Advanced Materials* **10**, 135-138 (1998).

50 Henderson, M. A. The interaction of water with solid surfaces: fundamental aspects revisited. *Surface Science Reports* **46**, 1-308, (2002).

51 Pan, J. M., Maschhoff, B., Diebold, U. & Madey, T. Interaction of water, oxygen, and hydrogen with TiO_2 (110) surfaces having different defect densities. *Journal of Vacuum Science & Technology A: Vacuum, Surfaces, and Films* **10**, 2470-2476 (1992).

52 Kumar, N., Kent, P. R., Wesolowski, D. J. & Kubicki, J. D. Modeling water adsorption on rutile (110) using van der Waals density functional and DFT+ U methods. *The Journal of Physical Chemistry C* **117**, 23638-23644 (2013).

53 Schaub, R. *et al.* Oxygen vacancies as active sites for water dissociation on rutile TiO_2 (110). *Physical Review Letters* **87**, 266104 (2001).

54 Gutiérrez Moreno, J. J., Fronzi, M., Lovera, P., O'Riordan, A. & Nolan, M. Stability of Adsorbed Water on TiO_2–TiN Interfaces. A First-Principles and Ab Initio Thermodynamics Investigation. *The Journal of Physical Chemistry C* **122**, 15395-15408, doi:10.1021/acs.jpcc.8b03520 (2018).

55 Kowalski, P. M., Meyer, B. & Marx, D. Composition, structure, and stability of the rutile TiO_2 (110) surface: Oxygen depletion, hydroxylation, hydrogen migration, and water adsorption. *Physical Review B* **79**, 115410 (2009).

56 Jung, J., Shin, H.-J., Kim, Y. & Kawai, M. Controlling water dissociation on an ultrathin MgO film by tuning film thickness. *Physical Review B* **82**, 085413 (2010).

57 Shin, H.-J. *et al.* State-selective dissociation of a single water molecule on an ultrathin MgO film. *Nature Materials* **9**, 442 (2010).

58 Song, Z., Fan, J. & Xu, H. Strain-induced water dissociation on supported ultrathin oxide films. *Scientific Reports* **6**, 22853 (2016).

59 Blöchl, P. E. Projector augmented-wave method. *Physical Review B* **50**, 17953-17979 (1994).

60 Kresse, G. & Joubert, D. From ultrasoft pseudopotentials to the projector augmented-wave method. *Physical Review B* **59**, 1758-1775 (1999).

61 Perdew, J. P. & Wang, Y. Accurate and simple analytic representation of the electron-gas correlation energy. *Physical Review B* **45**, 13244-13249 (1992).

62 Himmetoglu, B., Floris, A., Gironcoli, S. & Cococcioni, M. Hubbard- corrected DFT energy functionals: The LDA+ U description of correlated systems. *International Journal of Quantum Chemistry* **114**, 14-49 (2014).

63 Iwaszuk, A. & Nolan, M. Reactivity of sub 1 nm supported clusters:$(TiO_2)_n$ clusters supported on rutile TiO_2 (110). *Physical Chemistry Chemical Physics* **13**, 4963-4973 (2011).

64 Tang, W., Sanville, E. & Henkelman, G. A grid-based Bader analysis algorithm without lattice bias. *Journal of Physics: Condensed Matter* **21**, 084204 (2009).
65 M. Marlo, V. M. Density-functional study of bulk and surface properties of titanium nitride using different exchange-correlation functionals. *Physical Review B* **62** (2000).
66 Perron, H. *et al.* Optimisation of accurate rutile TiO_2(110), (100), (101) and (001) surface models from periodic DFT calculations. *Theoretical Chemistry Accounts* **117**, 565-574, doi:10.1007/s00214-006-0189-y (2007).
67 Stull, D. R. & Prophet, H. JANAF thermochemical tables. (DTIC Document, 1971).
68 Fronzi, M., Piccinin, S., Delley, B., Traversa, E. & Stampfl, C. Water adsorption on the stoichiometric and reduced CeO_2 (111) surface: a first-principles investigation. *Physical Chemistry Chemical Physics* **11**, 9188-9199 (2009).
69 Fronzi, M., Piccinin, S., Delley, B., Traversa, E. & Stampfl, C. CH_x adsorption (x= 1–4) and thermodynamic stability on the CeO_2 (111) surface: a first-principles investigation. *Rsc Advances* **4**, 12245-12251 (2014).
70 Sugizaki, Y., Ozawa, K. & Edamoto, K. Growth of ultrathin titanium oxide films on Ag(110). *Japanese Journal of Applied Physics* **56**, 085501, doi:10.7567/jjap.56.085501 (2017).
71 Papageorgiou, A. C. *et al.* Growth and Reactivity of Titanium Oxide Ultrathin Films on Ni(110). *The Journal of Physical Chemistry C* **111**, 7704-7710, doi:10.1021/jp067802m (2007).
72 Pan, X., Yang, M.-Q., Fu, X., Zhang, N. & Xu, Y.-J. Defective TiO_2 with oxygen vacancies: synthesis, properties and photocatalytic applications. *Nanoscale* **5**, 3601-3614 (2013).
73 Morgan, B. J. & Watson, G. W. A DFT + U description of oxygen vacancies at the TiO_2 rutile (110) surface. *Surface Science* **601**, 5034-5041 (2007).
74 Mattioli, G., Filippone, F., Alippi, P. & Bonapasta, A. A. Ab initio study of the electronic states induced by oxygen vacancies in rutile and anatase TiO 2. *Physical Review B* **78**, 241201 (2008).
75 Gutiérrez Moreno, J. J., doi:http://dx.doi.org/10.17172/NOMAD/2017.09.22-1.
76 Wendt, S. *et al.* Oxygen vacancies on TiO_2 (110) and their interaction with H_2O and O_2: A combined high-resolution STM and DFT study. *Surface Science* **598**, 226-245 (2005).
77 Perron, H. *et al.* Combined investigation of water sorption on TiO_2 rutile (1 1 0) single crystal face: XPS vs. periodic DFT. *Surface Science* **601**, 518-527 (2007).
78 Amtout, A. & Leonelli, R. Optical properties of rutile near its fundamental band gap. *Physical Review B* **51**, 6842-6851 (1995).
79 Nolan, M. & Tofail, S. A. The atomic level structure of the TiO_2-NiTi interface. *Physical Chemistry Chemical Physics* **12**, 9742-9750, doi:10.1039/c002562c (2010).

ACKNOWLEDGEMENTS

This work was supported by the Environmental Protection Agency UisceSense project (W-2015-MS-21). J.J.G.M. and W.L. acknowledge financial support from the National Natural Science Foundation of China under Grant No. 31770777, the Postdoctoral Science Foundation of China under Grant No. 802-011636 and the Startup Foundation for Peacock Talents, Shenzhen University. The authors wish to acknowledge the Paratera cloud server in China, DJEI/DES/SFI/HEA funded Irish Centre for High-End Computing (ICHEC) and the DECI-14 resource Bem based in Poland at WCSS with support from the PRACE aisbl for the provision of computational facilities and support.